A class of inhomogeneous shear models for seismic response of dams and embankments

Panos Dakoulas and George Gazetas

Department of Civil Engineering, Rensselaer Polytechnic Institute, Troy, N.Y. 12180, USA

Results of linear and nonlinear static analyses of gravity-induced stresses in several typical dam cross-sections, in conjunction with published experimental correlations of shear modulus versus confining pressure for a large variety of soils, reveal that the average shear modulus across the width of earth/rockfill dams may be expressed as a power m of depth, with m ranging from 0.35 to 0.90 and depending on material and geometric parameters. A general inhomogeneous shear beam model is developed to account for any possible such variation of modulus with depth. Perhaps somewhat surprisingly, closed-form analytical expressions are derived for natural frequencies, modal displacements, participation factors, and steady-state response functions for all values of the inhomogeneity factor m. Parametric results are presented in tabular and graphical form and conclusions are drawn of practical significance. Finally, a comprehensive comparative study is undertaken to investigate the validity of the inhomogeneous shear beam (SB) models. For five different dam cross-sections, each excited by four recorded accelerograms, it is shown that plane-strain finite-element analyses yield fundamental periods and peak displacements within the dam which are in very good accord with the predictions of a 'consistent' inhomogeneous SB model. A companion paper[1] extends the present work and focuses on seismic shear strains and seismic coefficients within dams and embankments.

INTRODUCTION

The shear beam (SB) model has been used extensively over the years to estimate the lateral seismic response of earth/rockfill dams and embankments,[2-7] its popularity stemming mainly from its simplicity. A number of rigorous studies[8-10] have largely corroborated one of the crucial assumptions of the SB model, namely that horizontal shear strains, shear stresses and displacements are essentially uniformly distributed across the width of the dam, and have moreover shown that the SB model yields natural periods and modal shapes which are quite realistic. These conclusions are also confirmed by the results of this and the companion paper.[1] To account for the dependence of soil stiffness on confining pressure, an improved version of the SB model has been developed which considers the (average across the width) shear modulus as increasing with the 2/3 power of the depth.[10,11] Direct and indirect evidence, including *in-situ* measurements of S-wave velocities and observations of the actual response of several dams[20-12] have shown the general validity of such a modulus variation with depth. Other researchers[13-15] have also suggested a shear modulus increasing with depth, although not quite as steeply as with the 2/3 power.

This paper first outlines the results of a comprehensive investigation on the factors influencing the variation of stiffness in earth and rockfill dams. It is concluded that the (average across the dam) shear modulus may be realistically considered as increasing with the m power of the depth z, where m may usually take values in the range $0.40 \leqslant m \leqslant 0.75$. Then an exact analytical solution is derived for free and forced vibrations of a truncated shear wedge (as sketched in Fig. 1) characterized by an arbitrary value of the power m. The third objective of the paper is to present the results of a comprehensive comparative study in which the seismic response of several dam sections are computed by plane finite-element (FE) and by inhomogeneous SB analysis. For each dam section the power m of the SB model is selected such that its modulus variation is consistent with the spatial variation of stiffness in the specific plane-strain model. It is concluded that such a 'compatible' inhomogeneous SB predicts fundamental periods and peak seismic displacements which are in a very close agreement with those computed with the corresponding FE models. The present study is further extended in a companion paper[1] which focuses on distribution of peak seismic shear strains and seismic coefficients in dams and embankments.

MODULUS VARIATION WITH DEPTH

While several (material, geometry and excitation related) factors influence the spatial distribution of effective shear moduli within a dam, it has been found in the course of our investigation that the average modulus, $G(z)$, over a horizontal plane at a depth z from the origin (Fig. 1), depends mainly on three factors:

(a) the dependence on confining pressure of the shear modulus G_e of each constituent material
(b) the size and the relative overall stiffness of the impermeable cohesive core
(c) the inclination of the slopes and the truncation ratio.

The effect of these factors on $G(z)$ is quantitatively illustrated in this section.

The shear modulus of a particular soil element at small levels of shear strain can be expressed as:

$$G_e = F(e, OCR) \cdot \sigma^{n}_{oct} \qquad (1)$$

where: σ_{oct} = the effective normal octahedral stress; and e

Accepted May 1985. Discussion closes December 1985.

0267-7261/85/040166-17$2.00

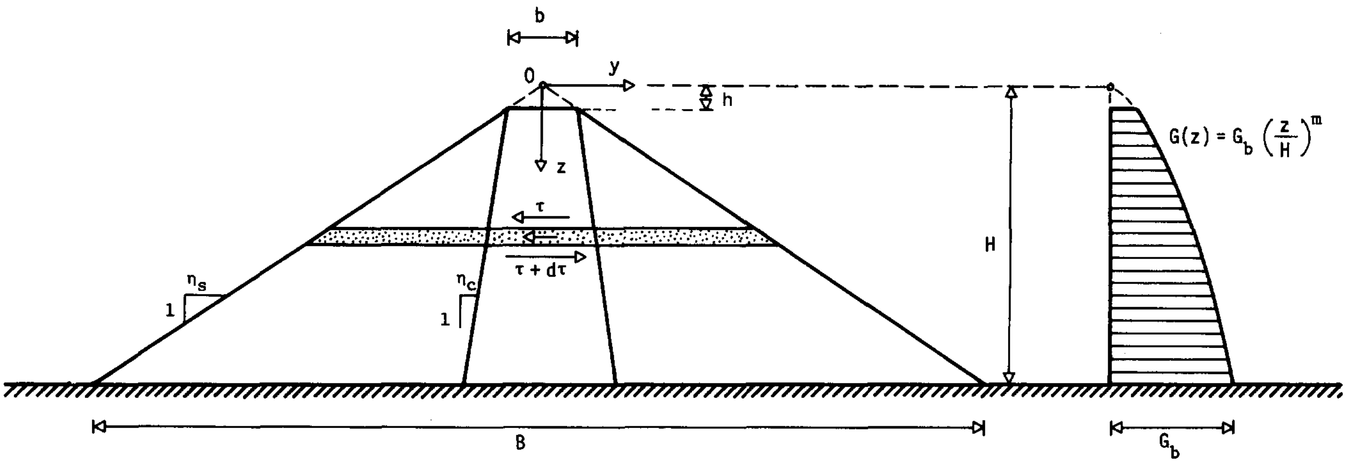

Fig. 1. Dam cross-section and distribution of shear modulus with depth

and OCR = the void ratio and apparent over-consolidation ratio of the particular element, respectively. The function F varies from soil to soil, monotonically increasing with decreasing e and increasing OCR. The dimensionless coefficient μ has been known to be about 0.50 for many laboratory tested soils, primarily clean sands and pure clays.[16,17] In the last decade, however, evidence which has accumulated from laboratory testing of a wide variety of real-life soils suggests that μ may take values anywhere between 0.35 and 0.90. A thorough literature survey produced an abundance of data, some of which is summarized in Table 1. This information can be utilized to make reasonably good estimates of μ for most materials to be used in the construction of dams and embankments.

An interesting recent development comes from the work of Stokoe and his co-workers[24,25] who studied the propagation of S and P waves through a large cubic sample of sand (each side = 2.1 m) subjected to (truly) triaxial states of (initial) stress. They found that the S wave velocity depends only on two of the principal stresses, in the direction of propagation and in the direction of particle motion. The principal stress in the out-of-plane direction, in which no shear-wave particle motion occurs, has practically no influence on the magnitude of the shear velocity. Hence, it appears that the element shear modulus could be expressed as:

$$G_e = F_*(e, OCR) \cdot \sigma_p^{\mu} \tag{2a}$$

where, for lateral vibration of dams as in Fig. 1,

$$\sigma_p = (\sigma_y + \sigma_z)/2 \tag{2b}$$

Note that under plane-strain conditions, as in the problem under study, σ_p would be equal to σ_{oct} if Poisson's ratio, ν, were equal to 0.50, but would slightly exceed σ_{oct} for the smaller values of ν that are realistic for most earth and rockfill dams.

Having established the likely range of μ values, parametric static finite-element (FE) analysis were conducted to determine the distribution of gravity-induced 'initial' stresses in cross-sections typical of dams and embankments. Numerous linear but also a few nonlinear analyses, assuming both 'single-lift' and 'multi-lift' construction, were performed. Most of the studied sections were idealized and made up of only one or two different zones, but some actual earth dam sections with known material properties (from the published literature) were also investigated.

A typical set of results is shown in Fig. 2 for a uniform 120 m high dam made up of material having properties similar to those of the silty gravelly sand zone of the Chatfield Dam.[26] Plotted in Fig. 2a are the distributions along the central vertical axis of the two in-plane principal stresses, σ_1 and σ_3, as derived from the nonlinear computer code FEADAM[27] assuming a 15-lift construction. Notice that while σ_1 increases essentially linearly with z, the rate of increase of σ_3 is much faster: $\sigma_3 \propto z^{1.50}$, approximately. Assuming that the shear modulus G_e of each element is given by equation (2) with $\mu = 0.50$ and that $F_*(e, OCR)$ remains constant throughout the dam, leads to element moduli, G_e, which are almost uniformly distributed in the horizontal direction but increase appreciably with depth. In fact, the average modulus G over a horizontal plane (across the dam), which is used in the SB model, increases with z as shown in Fig. 2b. The following general dimensionless expression can be fitted to this curve with reasonable accuracy:

$$G = G_b \zeta^m \tag{3}$$

Table 1. Summary of representative laboratory results on the dependence of shear modulus on confining pressure [*equation (1)*]

Type of Material	Type of Test	Reported μ Value for equation (1)	Reference
Angular and round grained sands	Resonant column	0.40–0.50	16–18
Normally consolidated clays	Resonant column; improved triaxial	0.50–0.60	17, 19
Compacted coarse gravel (D_{50} = 45 mm)	Special resonant column apparatus	0.38	20
Silty sand (D_{50} = 0.07 mm, 55% fines)	Resonant column; cyclic triaxial	0.60–0.90	21, 22
Silty sand (D_{50}0.02 mm, 80% fines)	Resonant column	0.77	23

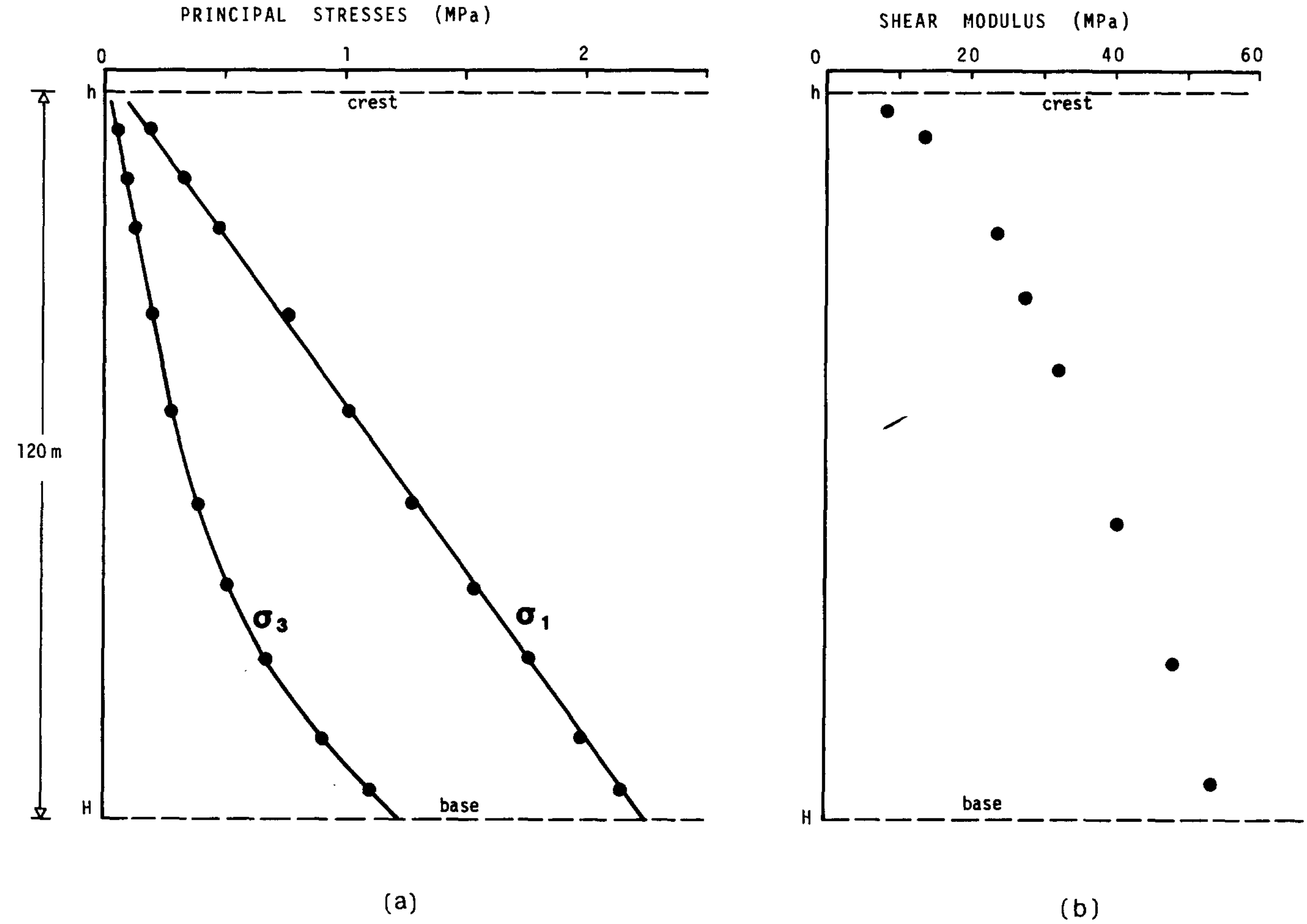

Fig. 2. Nonlinear static analysis of a 120 m high dam: (a) Distribution of principal stresses along the central axis; (b) Distribution with depth of the average shear modulus across the width

in which: $\zeta = z/H$, $G = G(\zeta)$ and G_b = the average shear modulus at the base of the dam ($\zeta = 1$). In this particular case, the best fit was achieved with $m \simeq 0.60 = \mu + 0.10$. (In fact a value of $m \simeq 0.70$ seemed to fit the near-the-crest portion of the curve and $m \simeq 0.57$ its lower half, with $m \simeq 0.60$ being the weighted average.)

It was concluded from such studies that, in general,

$$m = \mu + d \tag{4}$$

in which: μ is the power of equation (2) for the predominant constituent dam material, while d is depended primarily on the size and stiffness of the core as well as on the geometry of the embankment. Figure 3 summarizes the results of our parameter study in the form of simple graphs which can be used as a guide in selecting d, and hence m, in a variety of practical situations. It may be concluded that in most cases d is in the range of 0.05 to 0.20. Therefore, in view of the range of μ values depicted in Table 1, the exponent m of equation (3) is likely to attain values anywhere between 0.40 and 0.80. Hence the interest in developing a class of inhomogeneous SB models in which G varies according to equation (3) with any possible value of m.

INHOMOGENEOUS SB MODELS: LATERAL FREE VIBRATIONS

Referring to Fig. 1, the governing equation of motion is derived by considering the dynamic equilibrium of an infinitesimal body of volume b.dz.1 along with the elastic relationship between (average) shear stress and shear strain. For free undamped vibrations:

$$\rho \frac{\partial^2 u}{\partial t^2} = \frac{1}{z}\frac{\partial}{\partial z}\left[G(z) z \frac{\partial u}{\partial z}\right] \tag{5}$$

where $u(z,t)$ is the lateral horizontal displacement, and ρ the mass density of the soil.

By introducing the shear wave velocity at the base $C_b = \sqrt{[G_b \rho]}$ and utilizing equation (3), the above equat ion takes the form:

$$\frac{\partial^2 u}{\partial t^2} = \frac{C_b^2}{H^m}\cdot\frac{1}{z}\frac{\partial}{\partial z}\left(z^{m+1}\frac{\partial u}{\partial z}\right) \tag{6}$$

Setting

$$u(z,t) = U(z)e^{i\omega t} \tag{7}$$

and substituting into equation (6), leads to

$$z^2 U'' + (m+1) z U' + k^2 z^{2-m} U = 0 \tag{8}$$

where

$$k = \frac{\omega H^{m/2}}{C_b} \tag{9}$$

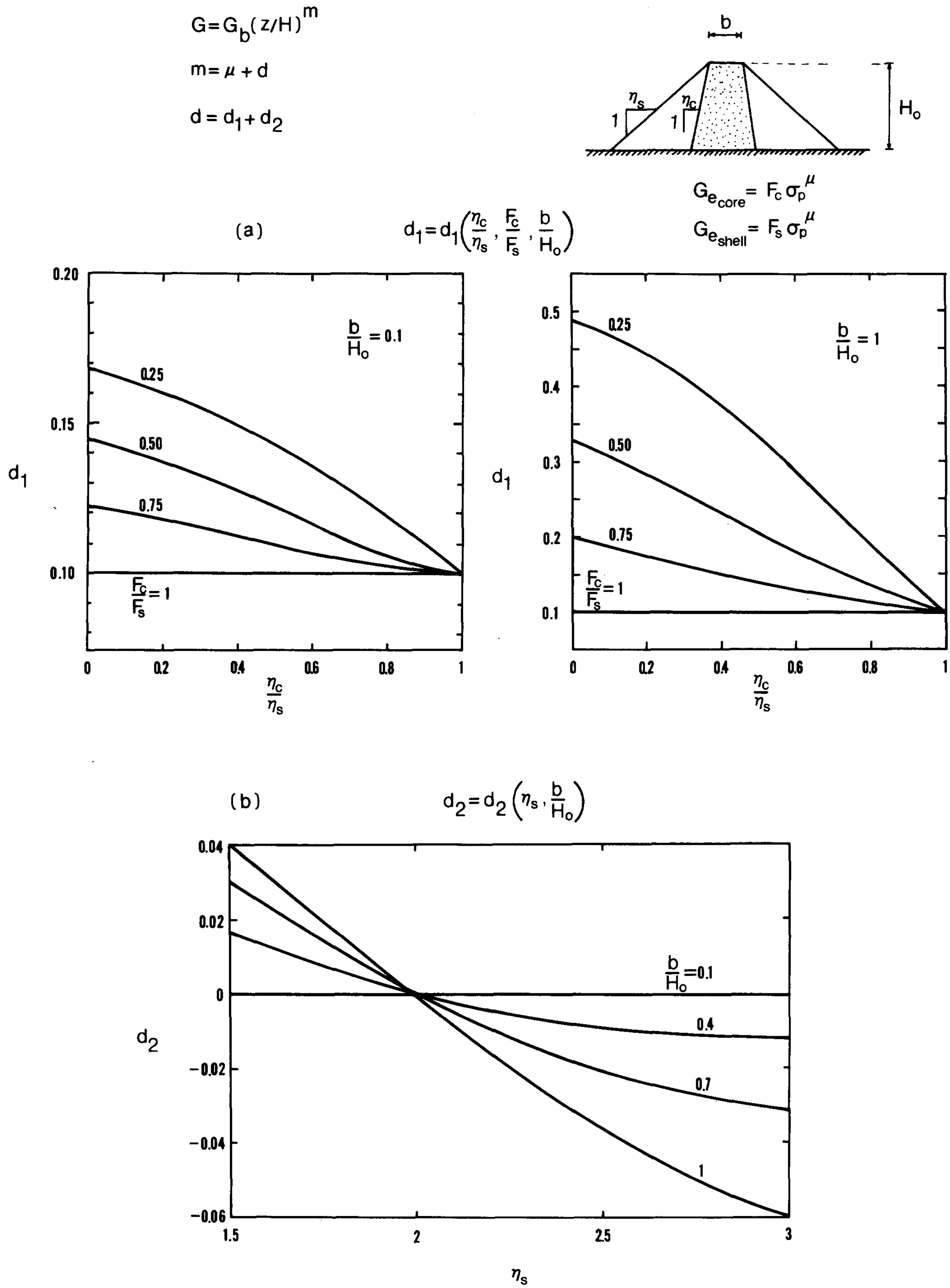

Fig. 3. Effect of core and dam geometry on the inhomogeneity parameter m

Equation (8) is a Bessel equation and its solution is

$$U(z)=z^{-m/2}\{AJ_q[k(1+q)z^{1-m/2}] + BY_q[k(1+q)z^{1-m/2}]\} \quad (10)$$

where J_q and Y_q are the Bessel functions of first and second kind, respectively, and of order

$$q=\frac{m}{2-m} \quad (11)$$

while A and B are integration constants.

Applying the boundary requirements for zero relative displacement at the base and zero shear stress at the crest yields, respectively,

$$H^{-m/2}\{AJ_q[k(1+q)H^{1-m/2}]+BY_q[k(1+q)H^{1-m/2}]\}=0 \quad (12a)$$

and

$$-\frac{G_b k}{H^m}\{AJ_{q+1}[k(1+q)h^{1-m/2} + BY_{q+1}[k(1+q)h^{1-m/2}]\}=0 \quad (12b)$$

from which, by eliminating A and B, one obtains the 'characteristic' relation

$$J_{q+1}(a\lambda^{1-m/2})Y_q(a)-Y_{q+1}(a\lambda^{1-m/2})J_q(a)=0 \quad (13)$$

in which

$$a=\frac{\omega H}{C_b}(1+q) \quad (14)$$

and λ is the truncation ratio:

$$\lambda=\frac{h}{H} \quad (15)$$

Equation (13) has a discretely infinite number of roots, $a_n=a_n(m)$, $n=1,2,\ldots$, which must be derived numerically. Substituting each of the a_n values in equation (10) leads to the following expression for the displacement shape at the nth vibration mode:

$$U_n(\zeta)=\zeta^{-m/2}N_q(a_n\zeta^{1-m/2}), \quad n=1,2,\ldots \quad (16)$$

where $N_p(\ )$ denotes the cylinder function:

$$N_{p(\ )}=Y_q(a_n)\cdot J_p(\ )-J_q(a_n)\cdot Y_p(\ ) \quad (17)$$

and $\zeta=z/H$.

NATURAL FREQUENCIES AND DISPLACEMENT SHAPES

The nth natural frequency and period of the dam expressed in terms of the shear wave velocity at the base are given by

$$\omega_n=\frac{a_n(2-m)}{2}\frac{C_b}{H} \quad \text{and} \quad T_n=\frac{4\pi}{a_n(2-m)}\frac{H}{C_b} \quad (18)$$

The values of a_n depend on the inhomogeneity m, for each value of truncation ratio $\lambda=h/H$. Tables 2–6 present the values of a_n for $n=1$–8, corresponding to five characteristic values of the inhomogeneity parameter ($m=0$, 1/2, 4/7, 2/3 and 1) and a wide range of truncation ratios. Small

Table 2. Roots a_n for coefficient of inhomogeneity m equal to 0

	mode n							
λ	1	2	3	4	5	6	7	8
0.00	2.405	5.520	8.654	11.792	14.931	18.071	21.212	24.352
0.03	2.409	5.541	8.703	11.880	15.068	18.262	21.464	24.670
0.05	2.416	5.576	8.783	12.016	15.265	18.527	21.797	25.074
0.10	2.448	5.726	9.096	12.510	15.949	19.403	22.866	26.335
0.15	2.501	5.948	9.525	13.153	16.807	20.473	24.148	27.829
0.20	2.574	6.233	10.048	13.917	17.809	21.711	25.622	29.536
0.25	2.668	6.580	10.666	14.804	18.963	23.131	27.305	31.484
0.30	2.786	6.994	11.388	15.831	20.293	24.763	29.239	33.718
0.35	2.930	7.485	12.231	17.024	21.833	26.651	31.474	36.300
0.40	3.107	8.067	13.222	18.421	23.637	28.859	34.086	39.315
0.45	3.323	8.763	14.400	20.078	25.771	31.471	37.175	42.880
0.50	3.588	9.605	15.818	22.070	28.336	34.608	40.883	47.161

Table 3. Roots a_n for coefficient of inhomogeneity m equal to 1/2

	mode n							
λ	1	2	3	4	5	6	7	8
0.00	2.903	6.033	9.171	12.310	15.451	18.591	21.733	24.874
0.03	2.910	6.078	9.295	12.549	15.834	19.141	22.942	26.271
0.05	2.921	6.148	9.465	12.844	16.262	19.707	23.478	26.794
0.10	2.974	6.415	10.035	13.740	17.488	21.260	25.245	29.380
0.15	3.055	6.775	10.727	14.769	18.849	22.950	27.018	31.210
0.20	3.164	7.209	11.521	15.919	20.351	24.801	29.710	33.534
0.25	3.301	7.718	12.422	17.208	22.025	26.857	32.394	36.467
0.30	3.468	8.309	13.449	18.666	23.911	29.170	34.852	49.706
0.35	3.671	8.997	14.630	20.334	26.064	31.807	37.556	43.310
0.40	3.915	9.802	16.001	22.266	28.555	34.855	41.162	47.472
0.45	4.212	10.757	17.614	24.535	31.478	38.432	45.391	52.354
0.50	4.574	11.903	19.544	27.245	34.967	42.699	50.437	58.177

Table 4. Roots a_n for coefficient of inhomogeneity m equal to 4/7

λ	mode n 1	2	3	4	5	6	7	8
0.00	2.999	6.133	9.273	12.413	15.554	18.695	21.836	24.977
0.03	3.007	6.185	9.417	12.694	16.006	19.343	22.699	26.068
0.05	3.020	6.264	9.610	13.026	16.486	19.975	23.482	27.001
0.10	3.076	6.557	10.234	14.005	17.822	21.664	25.520	29.386
0.15	3.164	6.945	10.980	15.110	19.282	23.475	27.680	31.893
0.20	3.280	7.409	11.827	16.336	20.882	25.447	30.021	34.602
0.25	3.426	7.950	12.784	17.704	22.657	27.627	32.605	37.588
0.30	3.604	8.577	13.871	19.247	24.653	30.074	35.502	40.935
0.35	3.818	9.304	15.118	21.009	26.927	32.858	38.797	44.739
0.40	4.077	10.154	16.564	23.046	29.553	36.073	42.599	49.129
0.45	4.389	11.159	18.264	25.436	32.633	39.840	47.054	54.271
0.50	4.771	12.366	20.295	28.289	36.305	44.332	52.365	60.400

Table 5. Roots a_n for coefficient of inhomogeneity m equal to 2/3

λ	mode n 1	2	3	4	5	6	7	8
0.00	3.142	6.283	9.425	12.566	15.708	18.850	21.991	25.133
0.03	3.150	6.346	9.604	12.918	16.275	19.661	23.070	26.492
0.05	3.165	6.439	9.831	13.307	16.834	20.393	23.972	27.564
0.10	3.229	6.772	10.539	14.412	18.335	22.285	26.251	30.226
0.15	3.327	7.203	11.364	16.631	19.943	24.277	28.624	32.979
0.20	3.455	7.712	12.291	16.969	21.688	26.426	31.176	35.933
0.25	3.614	8.301	13.331	18.455	23.614	28.791	33.979	39.171
0.30	3.807	8.980	14.508	20.124	25.773	31.437	37.112	42.790
0.35	4.039	9.765	15.854	22.025	28.226	34.442	40.667	46.895
0.40	4.318	10.682	17.412	24.220	31.055	37.904	44.762	51.623
0.45	4.655	11.764	19.241	26.791	34.368	41.957	49.555	57.155
0.50	5.065	13.061	21.424	29.857	38.315	46.784	55.262	63.741

Table 6. Roots a_n for coefficients of inhomogeneous m equal to 1.0

λ	mode n 1	2	3	4	5	6	7	8
0.00	3.832	7.016	10.174	13.324	16.471	19.616	22.760	25.904
0.03	3.849	7.155	10.594	14.153	17.791	21.477	25.194	28.931
0.05	3.875	7.330	11.012	14.842	18.752	22.706	26.686	30.683
0.10	3.981	7.879	12.145	16.568	21.060	25.581	30.133	34.693
0.15	4.130	8.527	13.360	18.342	23.385	28.457	33.545	38.644
0.20	4.319	9.261	14.677	20.232	25.841	31.477	37.127	42.785
0.25	4.547	10.088	16.126	22.294	28.511	34.752	41.005	47.267
0.30	4.819	11.027	17.745	24.586	31.472	38.380	45.299	52.225
0.35	5.141	12.102	19.581	27.176	34.813	42.470	50.138	57.813
0.40	5.524	13.348	21.693	30.150	38.646	47.161	55.685	64.216
0.45	5.983	14.811	24.163	33.621	43.117	52.630	61.152	71.680
0.50	6.540	16.558	27.102	37.747	48.428	59.125	69.831	80.542

values of λ (0.02 to 0.10) are typical of earth and rockfill dams, whereas large values (0.20 to 0.50) are typical of embankments.

Alternatively, ω_n and T_n can be rewritten in terms of the average shear wave velocity, $\bar{C}$, of the dam:

$$\bar{C}=\frac{\int_{\lambda}^{1} C(\zeta)\zeta \,d\zeta}{\int_{\lambda}^{1} \zeta \,d\zeta}=\frac{4}{4+m}\,\frac{1-\lambda^{2+m/2}}{1-\lambda^2}\,C_b \tag{19}$$

The corresponding expressions for the fundamental period T_1 and the nth natural frequency ω_n are given in Table 7, along with the expressions for the modal displacement shape and the modal participation factor, for $\lambda=0.0$ (typical for tall earth and rockfill dams). Also given in this table are the formulae deduced from the general expressions for four characteristic values of the inhomogeneity parameter: $m=0$ (homogeneous), $m=1/2$, $m=2/3$ and $m=3/4$.

To further illustrate the effects of inhomogeneity on the dynamic characteristics of dams and embankments Figs. 4 and 5 contrast the natural periods T_n of five inhomogeneous dams with the corresponding periods T_{n0} of a homogeneous dam having the same height and average shear-wave velocity. Specifically, Fig. 4 plots as a function of m the ratio T_n/T_{n0} for $n=1$–4. For $\lambda=0$ (Fig. 4a), the degree of inhomogeneity has a negligible effect on the first mode (difference less than 2%), but it may affect

Table 7. Analytical results for dams with $G=G_b\zeta^m$ and $\lambda=0$ (typical for all earth/rock-fill dams)

Factor of Inhomogeneity m	Fundamental Period $T_1(\bar{C}/H)$	nth Natural Circular Freq. $\omega_n(H/\bar{C})$	nth Mode Displacement Shape U_n	nth Mode Participation Factor P_n	Acceleration Amplification Function $AF(\zeta)$	Crest Amplification Function
m (general expression)	$\dfrac{16\pi}{(4+m)(2-m)a_1}$	$\dfrac{(4+m)(2-m)a_n}{8}$	$\zeta^{-m/2}J_q[a_n\zeta^{1-m/2}]$	$\dfrac{2}{a_n}\dfrac{1}{J_{q+1}(a_n)}$	$\zeta^{-m/2}\dfrac{J_q(a\zeta^{1-m/2})}{J_q(a)}$	$\left(\dfrac{a}{2}\right)^q\dfrac{1}{\Gamma(q+1)J_q(a)}$
0 (homogeneous)	2.613	$a_n(0)$	$J_0[a_n(0)\zeta]$	$\dfrac{2}{a_n(0)}\dfrac{1}{J_1[a_n(0)]}$	$\dfrac{J_0(a\zeta)}{J_0(a)}$	$\dfrac{1}{J_0(a)}$
1/2	2.565	$0.843a_n(1/2)$	$\zeta^{-1/4}J_{1/3}[a_n(1/2)\zeta^{3/4}]$	$\dfrac{2}{a_n(1/2)}\dfrac{1}{J_{4/3}[a_n(1/2)]}$	$\zeta^{-1/4}\dfrac{J_{1/3}(a\zeta^{3/4})}{J_{1/3}(a)}$	$0.8888\dfrac{a^{1/3}}{J_{1/3}(a)}$
2/3	2.571	$0.788n\pi$	$\zeta^{-2/3}\sin[n\pi(1-\zeta^{2/3})]$	$\dfrac{2}{n\pi}$	$\zeta^{-2/3}\dfrac{\sin(a\zeta^{2/3})}{\sin a}$	$\dfrac{a}{\sin a}$
3/4	2.579	$0.742a_n(3/4)$	$\zeta^{-3/8}J_{3/5}[a_n(3/4)\zeta^{5/8}]$	$\dfrac{2}{a_n(3/4)}\dfrac{1}{J_{8/5}[a_n(3/4)]}$	$\zeta^{-3/8}\dfrac{J_{3/5}(a\zeta^{5/8})}{J_{3/5}(a)}$	$0.7384\dfrac{a^{3/5}}{J_{3/5}(a)}$

$a_n=a_n(m)$ has been tabulated in Tables 2–6; $q=m/(2-m)$; $a=\omega H(1+q)/C_b$; $\Gamma(\ )$ denotes the Gamma function

appreciably the higher modes. For example, for $m=2/3$, the fourth natural period is about 20% higher than the same period of the homogeneous dam. On the contrary, for $\lambda=0.5$ (Fig. 4) the effect inhomogeneity on the natural periods appears to be negligible, especially for the higher modes. In Fig. 5 plotted *versus* m is the ratio T_n/T_1, $n=1$–4. It is evident that this ratio decreases with increasing m, i.e. the consecutive natural periods get closer to each other in the more inhomogeneous earth dams. Naturally, of course, this effect is barely distinguishable for $\lambda=0.50$.

The effect of the type of inhomogeneity on the first four modal displacement shapes is portrayed in Fig. 6 for $m=0$, 1/2, 4/7, 2/3 and 1. Only results for $\lambda=0.0$ are shown, since the differences between shapes are negligible for $\lambda=0.50$. It is observed that for each and every mode the homogeneous model does not predict as sharp a 'deamplification' with depth as the one computed for dams with $m>0$ – a phenomenon previously noticed by Gazetas[10 11] for the particular case of $m=2/3$. Dams with large values of m deform almost like uniform 'flexural' beams despite the fact that only shear deformations take place. This apparent flexural behaviour is particularly strong when $m=1$ (strongly inhomogeneous dam). Notice, nonetheless, that the range of m values usually expected in practice ($0.40\leqslant m\leqslant 0.75$), the modal displacements shapes are not sensitive to small changes in m. Thus, uncertainties in assessing the appropriate value of m in practical situations are not likely to influence the analysis to a very significant degree.

RESPONSE TO SEISMIC BASE EXCITATION

For a synchronous (in-phase) oscillation of the rigid base described through the acceleration $\ddot{u}=\ddot{u}_g(t)$ in the y direction, the governing equation of motion takes the form

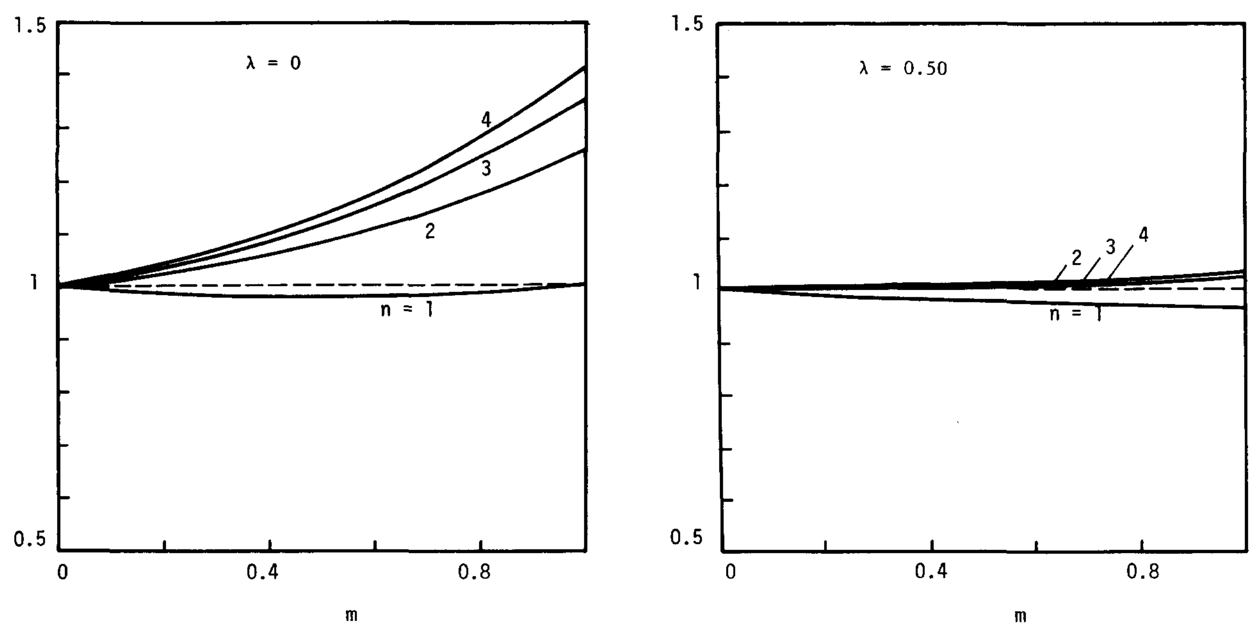

Fig. 4. Effect of inhomogeneity on the ratio of the natural periods of the inhomogeneous and homogeneous dams for: (a) $\lambda=0$ and (b) $\lambda=0.50$

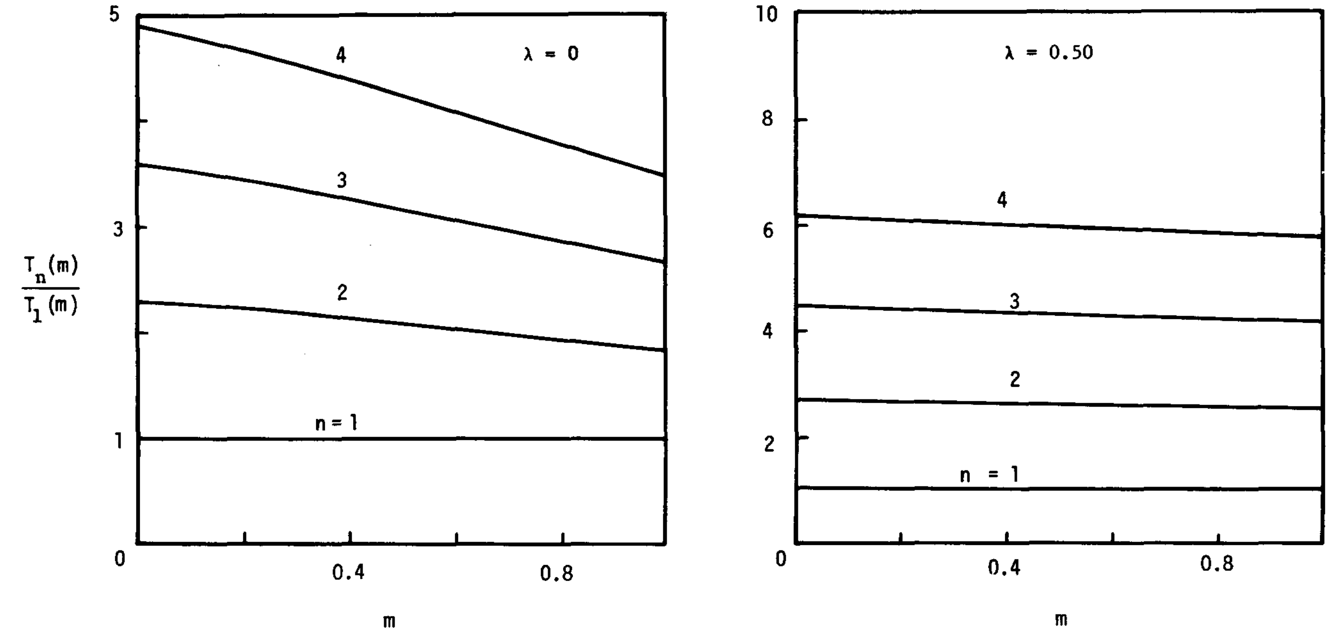

Fig. 5. Effect of inhomogeneity on the ratio of the nth natural period to the fundamental period for (a) $\lambda=0$ and (b) $\lambda=0.50$

$$\frac{1}{z}\frac{\partial}{\partial z}\left[C^2(z)\cdot z\frac{\partial u}{\partial z}\right]=\ddot{u}+\ddot{u}_g \tag{21}$$

in which $u=u(z,t)$ is displacement at depth z, relative to the base. The orthogonality condition (which, as easily shown, is satisfied in this case) allows using modal superposition. Hence, $u(z,t)$ is obtained as a summation of a discretely infinite number of displacement histories, corresponding to each of the natural frequencies of the dam:

$$u(z,t)=\sum_{n=1}^{\infty} P_n\cdot U_n(z)\cdot D_n(t) \tag{22}$$

where P_n is the participation factor of the nth mode

$$P_n=\frac{\int_{\lambda}^{1}\zeta U_n(\zeta)\,\mathrm{d}\zeta}{\int_{\lambda}^{1}\zeta U_n^2(\zeta)\,\mathrm{d}\zeta}=\frac{2}{a_n}\frac{N_{q+1}(a_n)}{N_{q+1}^2(a_n)-\lambda^{2-m}N_q^2(a_n\lambda^{1-m/2})} \tag{23}$$

and $D_n(t)$ is the reponse of a single degree of freedom system having frequency ω_n and damping β_n:

$$D_n(y)=\frac{1}{\omega_n^*}\int_0^t \ddot{u}_g(\tau)e^{-\beta_n\omega_n(t-\tau)}\sin\omega_n^*(t-\tau)\cdot\mathrm{d}\tau \tag{24}$$

in which $\omega_n^*=\omega_n(1-\beta_n^2)^{1/2}$. Expressions for P_n of several inhomogeneous dams are depicted in Table 7, for $\lambda=0.0$.

The absolute acceleration at a depth z is $\ddot{u}+\ddot{u}_g$. Making use of equation (22) $\ddot{u}_a$ is found equal to

$$\ddot{u}_a(z,t)=\sum_{n=1}^{\infty}P_nU_n(z)D_{an}(t)+\ddot{u}_g\left[1-\sum_{n=1}^{\infty}P_nU_n(z)\right] \tag{25}$$

where D_{an} is the expression

$$D_{an}=\frac{1-2\beta_n^2}{(1-\beta_n^2)^{1/2}}\cdot\omega_n\int_0^t\ddot{u}_g(\tau)e^{-\beta_n\omega_n(t-\tau)}\sin\omega_n^*(t-\tau)\,\mathrm{d}\tau+2\beta_n\omega_n\int_0^t\ddot{u}_g(\tau)e^{-\beta_n\omega_n(t-\tau)}\cos\omega_n^*(t-\tau)\,\mathrm{d}\tau \tag{26}$$

To evaluate displacements, the first few terms of the series (usually 3 or 4) are sufficient. The absolute acceleration, however, demands a larger number of terms (about 10 or more) as convergence of the series to the exact value of $\ddot{u}_a$ is slower.

It is of interest to focus on the displacement modal participation defined as the product of the participation factor times the respective modal displacement shape:

$$\Phi_n=\Phi_n(z)=P_nU_n(z) \tag{27}$$

Fig. 7 plots the variation of the Φ_n value at the crest of the dam, $\Phi_n(h)$, as a function of the truncation ratio λ, and the inhomogeneity parameter m, for $n=1$–8. Notice that for $\lambda=0$, while in dams with $m=2/3$ the value of $|\Phi_n|$ at the crest remains constant (independent of n) equal to 2, smaller values of m lead to $|\Phi_n|$ values which decrease monotonically with increasing mode number n. In the extreme case of a homogeneous model ($m=0$): $|\Phi_1|\simeq 1.61$, $|\Phi_2|\simeq 1.07$, $|\Phi_3|\simeq 0.85$, $|\Phi_4|\simeq 0.73$, and so on. Consequently, one should expect that, in general, the relative contribution of higher modes on the near-crest response will increase with increasing degree of inhomogeneity. This has indeed been evidenced in both the results of acceleration time-history analyses and the steady-state acceleration transfer functions to harmonic base excitation presented in the sequel (Fig. 8a).

STEADY-STATE RESPONSE TO HARMONIC BASE MOTION

It is of interest to show that a closed-form analytical

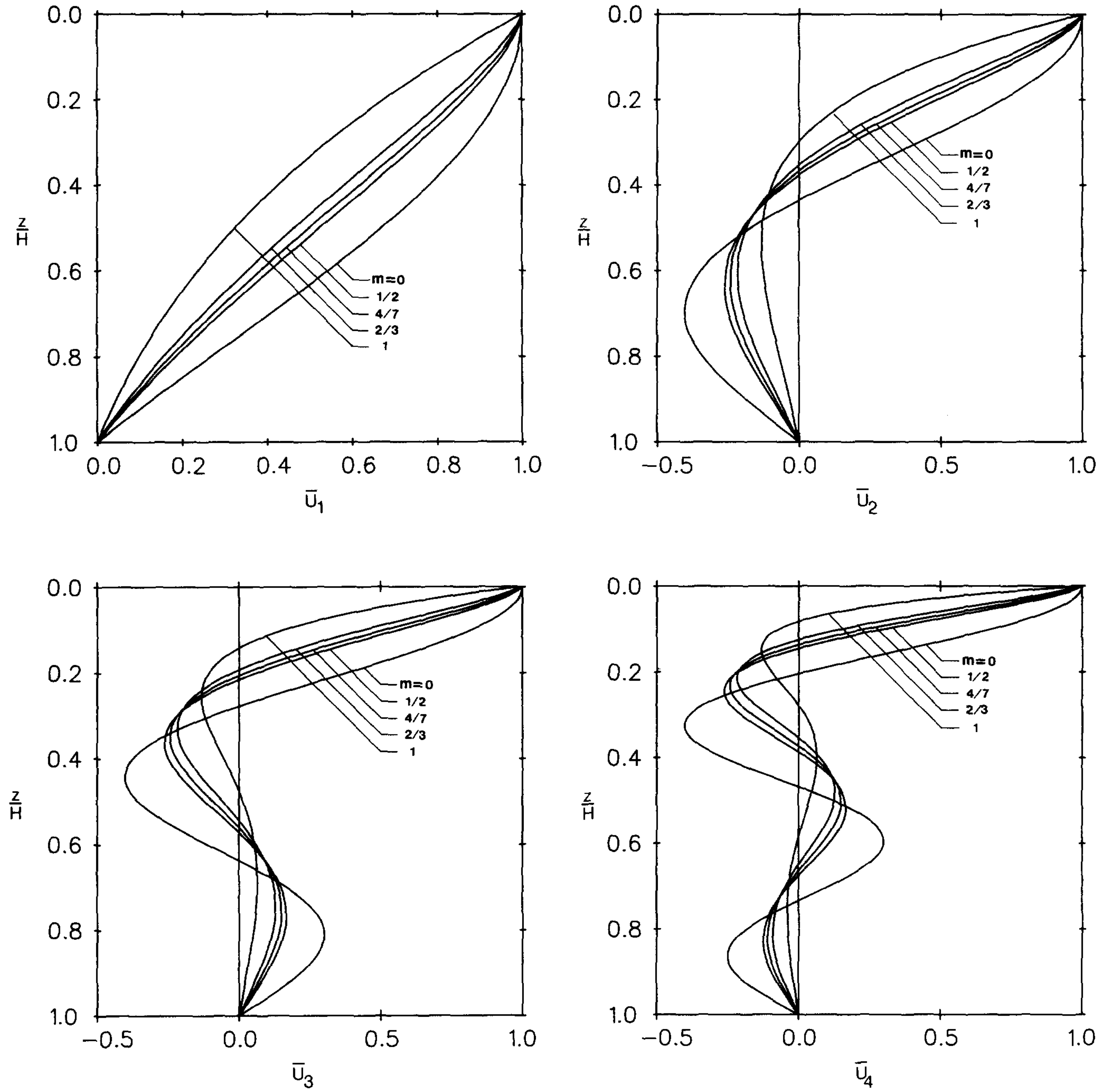

Fig. 6. Displacement modal shapes for five values of the inhomogeneity parameter (m=0, 1/2, 4/7, 2/3 and 1)

expression can be derived for steady-state displacements and accelerations arising from a harmonic base excitation. Indeed, equation (21) yields for the relative displacement $u(\zeta;t)=u(\zeta)\cdot e^{i\omega t}$:

$$\frac{u(\zeta)}{u_g}=\zeta^{-m/2}\cdot\frac{J_{q+1}(a\lambda^{1-m/2})Y_q(a\zeta^{1-m/2})-Y_{q+1}(a\lambda^{1-m/2})J_q(a\zeta^{1-m/2})}{J_{q+1}(a\lambda^{1-m/2})Y_q(a)-Y_{q+1}(a\lambda^{1-m/2})J_q(a)}-1 \qquad (28)$$

in which

$$a=\frac{\omega H}{C_b^*}(1+l) \qquad (29)$$

Equation (28) is valid for both real and $C_b^*=C_b$ (appropriate for cases with material damping = 0) and complex $C_b^*=C_b\sqrt{(1+2i\beta)}$ (for cases with material hysteretic damping ratio = β).

From equation (28) the transfer function of the absolute acceleration, $\ddot{u}+\ddot{u}_g$, usually named 'amplification' function, is determined:

$$AF(\zeta)=\frac{\ddot{u}(\zeta)+\ddot{u}_g}{\ddot{u}_g}=\frac{u(\zeta)}{u_g}+1 \qquad (30)$$

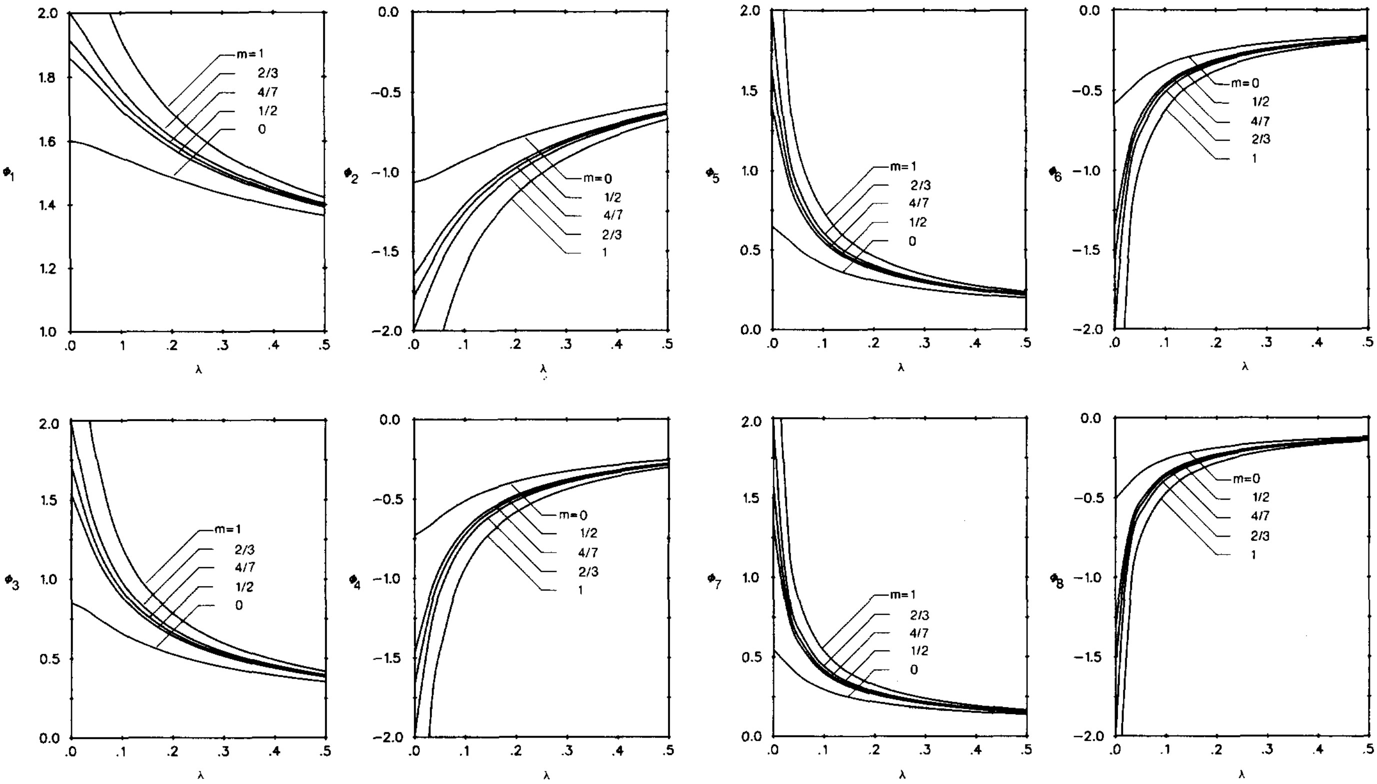

Fig. 7. Crest displacement modal participation $[\phi_n(0)=P_nU_n(0)]$ versus truncation ratio for the first 8 modes ($m=0$, 1/2, 4/7, 2/3 and 1)

Of special interest is the 'amplification' at the crest ($\zeta=\lambda$):

$$AF(\lambda)=\frac{2}{\pi\alpha\lambda}\left[J_{q+1}(a\lambda^{1-m/2})Y_q(a)-J_q(a)Y_{q+1}(a\lambda^{1-m/2})\right]^{-1} \tag{31}$$

Again, for tall dams ($\lambda\to 0$) equations (20) and (31) simplify, respectively, to

$$AF(\zeta)_{\lambda=0}=\zeta^{-m/2}\frac{J_q(a\zeta^{1-m/2})}{J_q(a)} \tag{32}$$

Table 8. Characteristics of the five dams used

Dam	Height (m)	Average S-wave Velocity (m/s)	C_{core}/C_{shell}	λ	Inhomogeneity Parameter m	T_1 (s) SB	T_1 (s) FE	Error
A	40	200	1.00	0.043	0.57	0.534	0.56	4.6
B	80	245	1.00	0.027	0.57	0.860	0.904	4.8
C	120	280	1.00	0.027	0.57	1.129	1.187	4.9
D	120	280	0.72	0.027	0.63	1.129	1.211	6.7
E	120	280	0.50	0.027	0.63	1.129	1.283	12.0

Table 9. The four earthquake records used

Earthquake	M	Record	Component	R (km)	Peak values of: Acceleration cm/sec^2	Peak values of: Velocity cm/sec	Peak values of: Displacement cm
Eureka (1954)	6.5	Eureka Federal Building	N79E	24.0	196.2*	22.8	10.9
Imperial Valley (1940)	6.7	El Centro	S00E	9.3	196.2*	19.2	6.24
San Fernando (1971)	6.4	1901 Ave. of the Stars Subbasement Los Angeles	N46W	39.8	196.2*	22.3	16.3
Kern County (1952)	7.7	Taft Lincoln School Tunnel	N21E	43.0	196.2*	20.2	8.6

* All records have been normalized to a 0.20 g peak acceleration

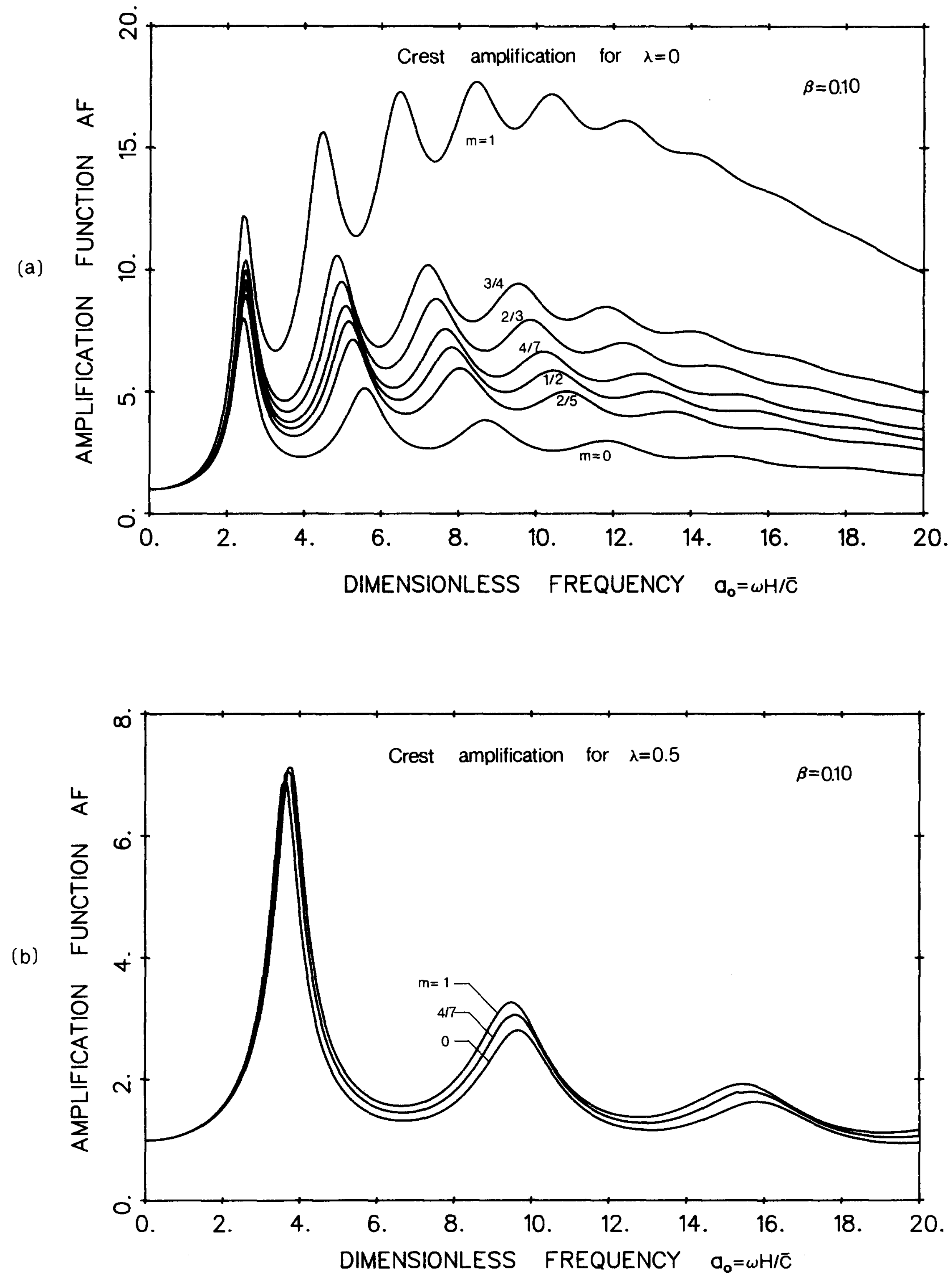

Fig. 8. Steady-state response to harmonic excitation: crest amplification of inhomogeneous and homogeneous dams for (a) $\lambda = 0$ and (b) $\lambda = 0.50$

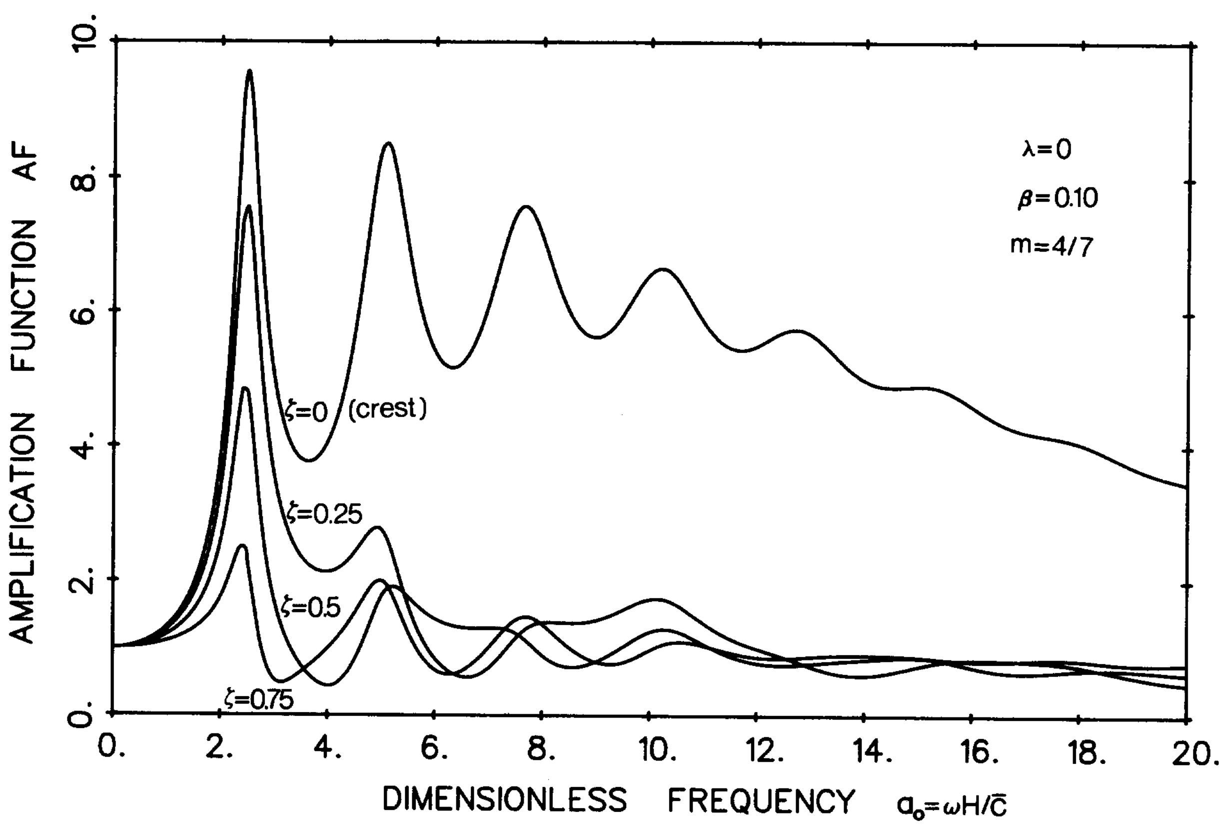

Fig. 9. Typical amplification functions at various depths in an inhomogeneous dam ($m=4/7$)

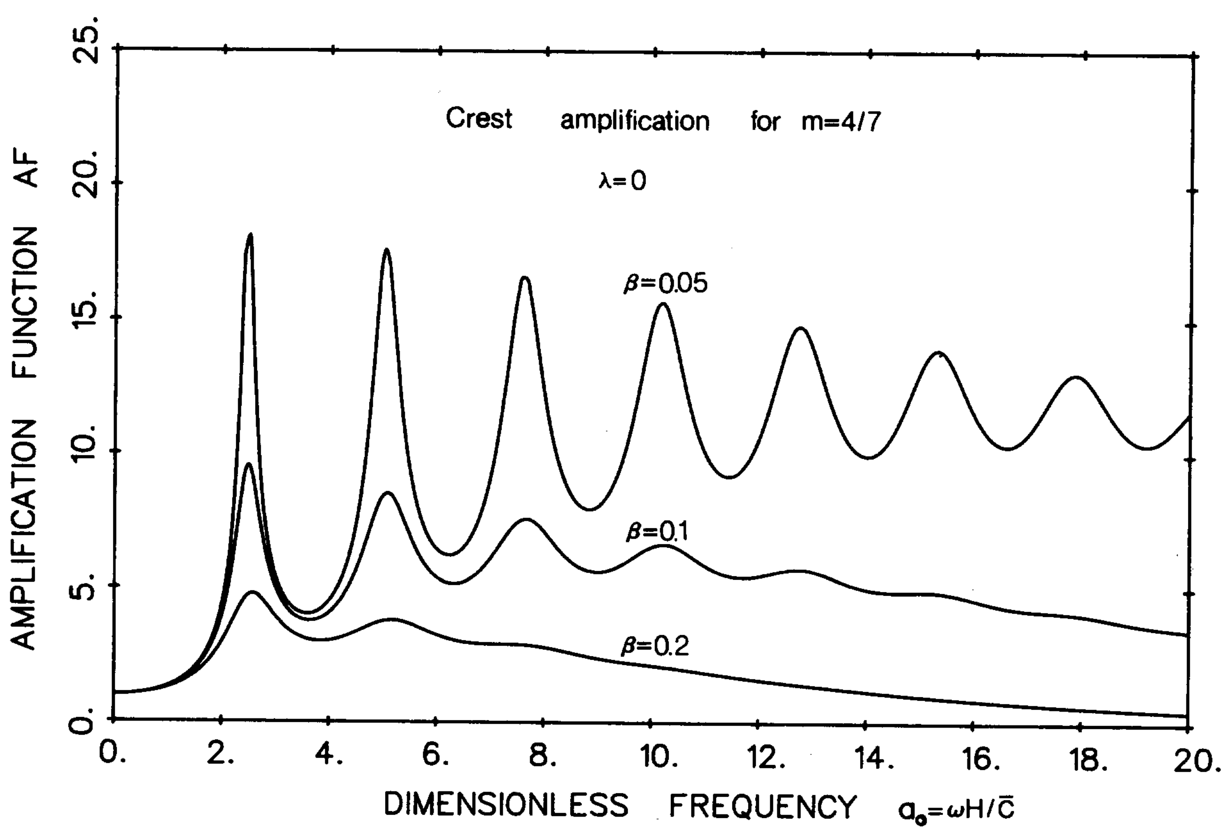

Fig. 10. Effect of hysteretic damping ratio on crest amplification for a typical inhomogeneous dam ($m=4/7$)

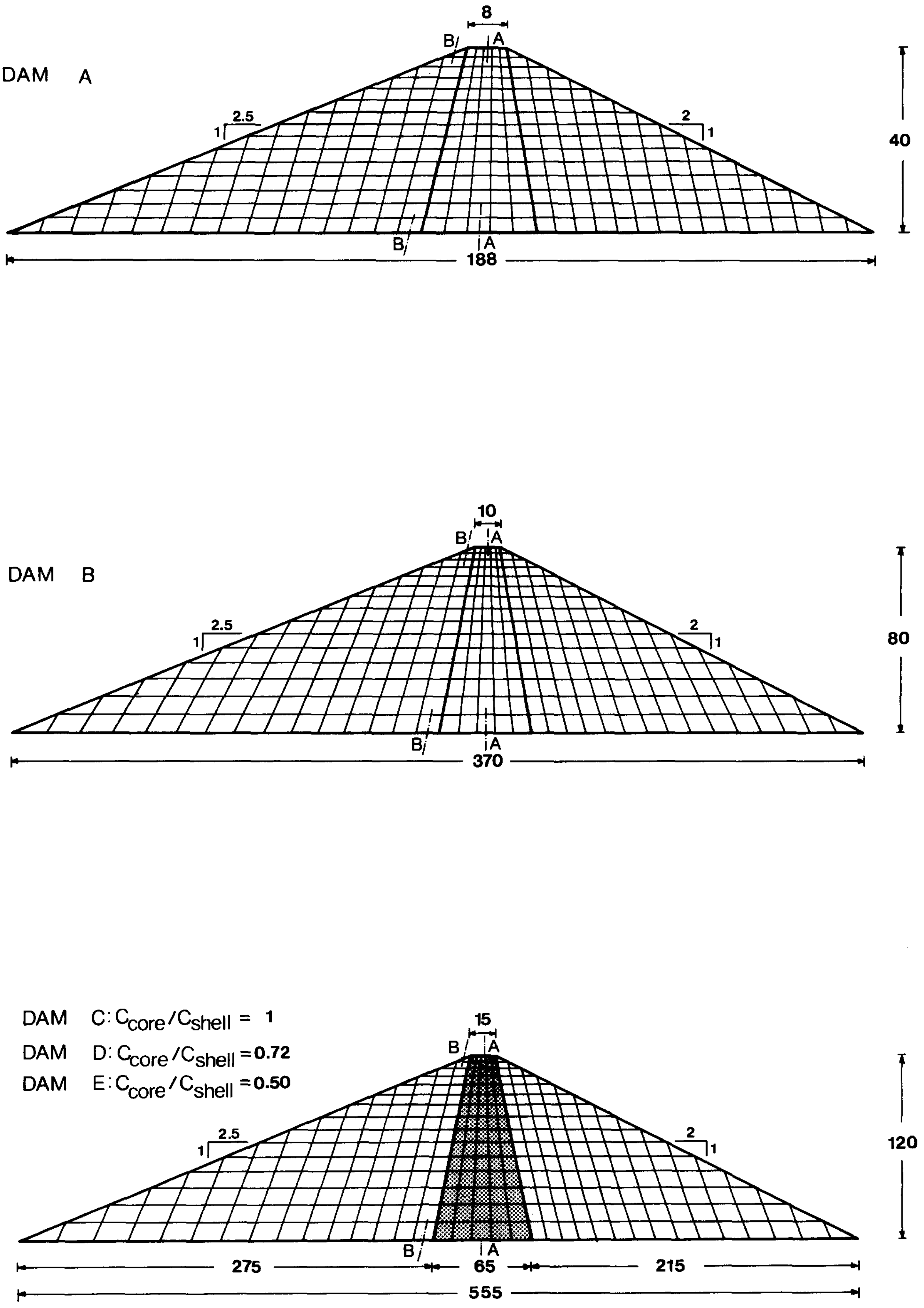

Fig. 11. Geometry, material properties and FE discretization of the five dams studied

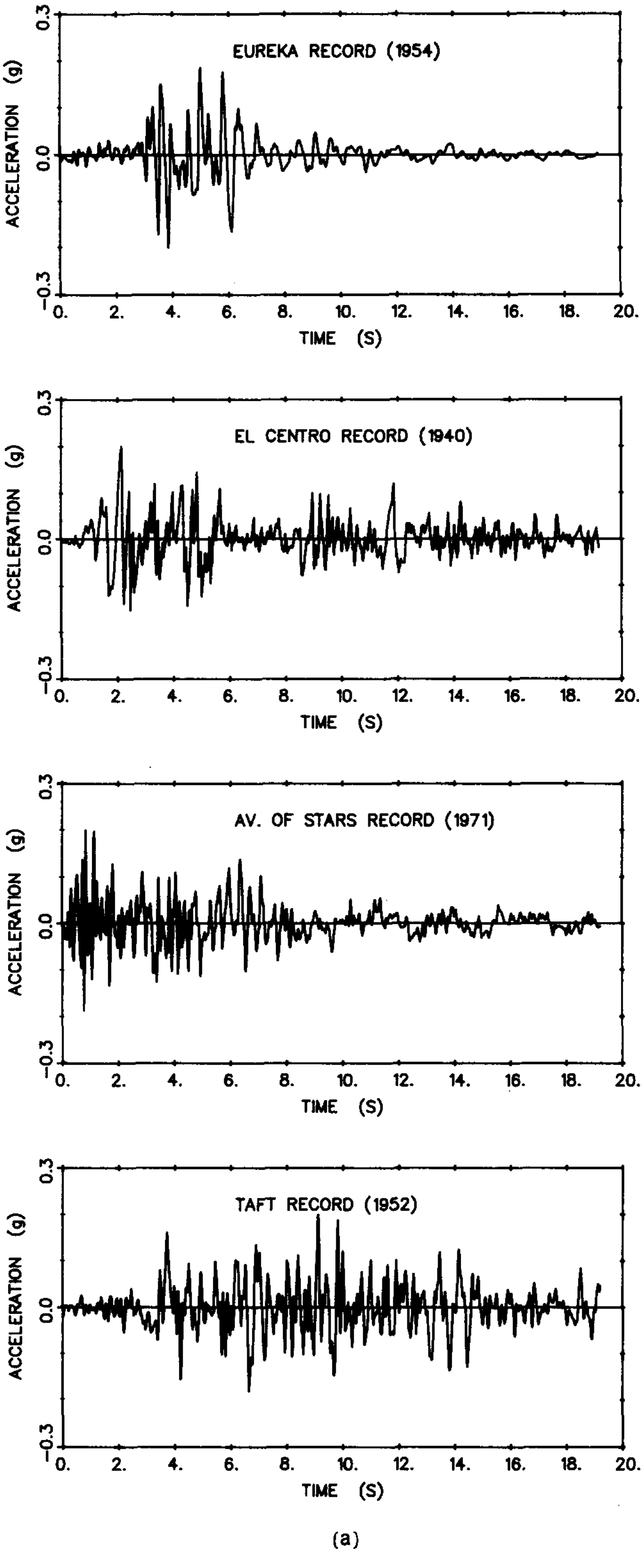

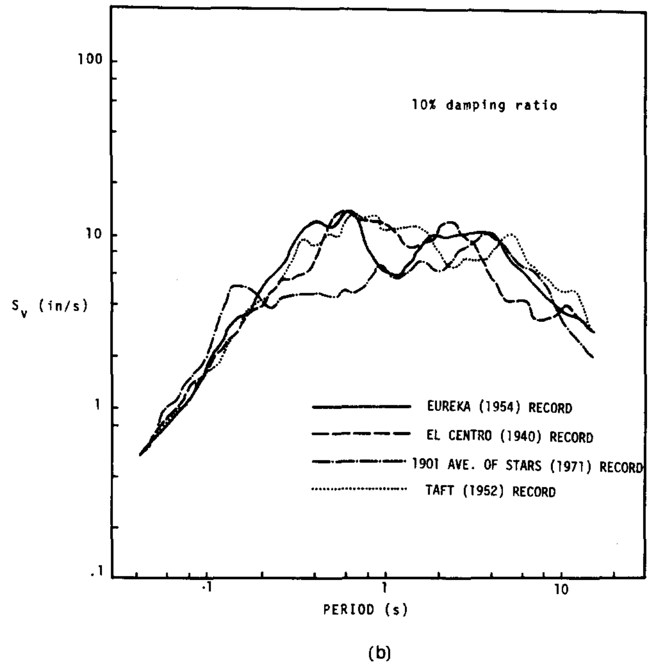

Fig. 12. (a) Scaled acceleration time histories of the four earthquakes. (b) Pseudo-velocity spectra of the four scaled records (damping ratio $\beta = 0.10$)

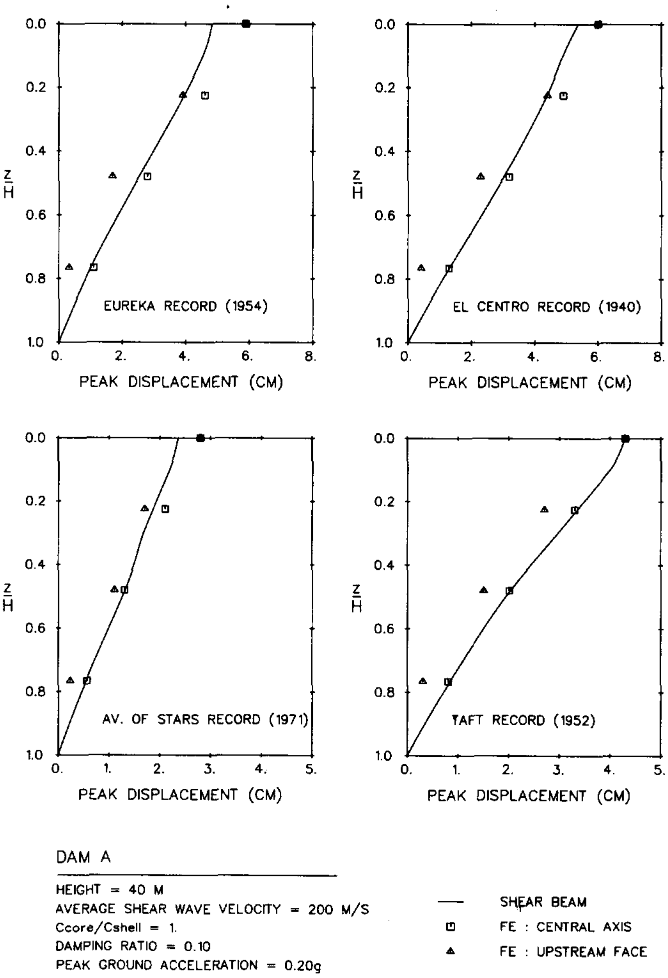

Fig. 13. Dam A: Distribution with depth of peak displacements from SB and FE analyses

and

$$AF(0)_{\lambda=0} = \left(\frac{a}{2}\right)^q [\Gamma(q+1) \cdot J_q(a)]^{-1} \tag{33}$$

in which $\Gamma(\ )$ denotes the Gamma function.

Notice that Table 7 depicts the foregoing general expressions for $AF(\zeta)$ and $AF(0)$, as well as the special expressions for $m = 0$, 1/2, 2/3 and 3/4.

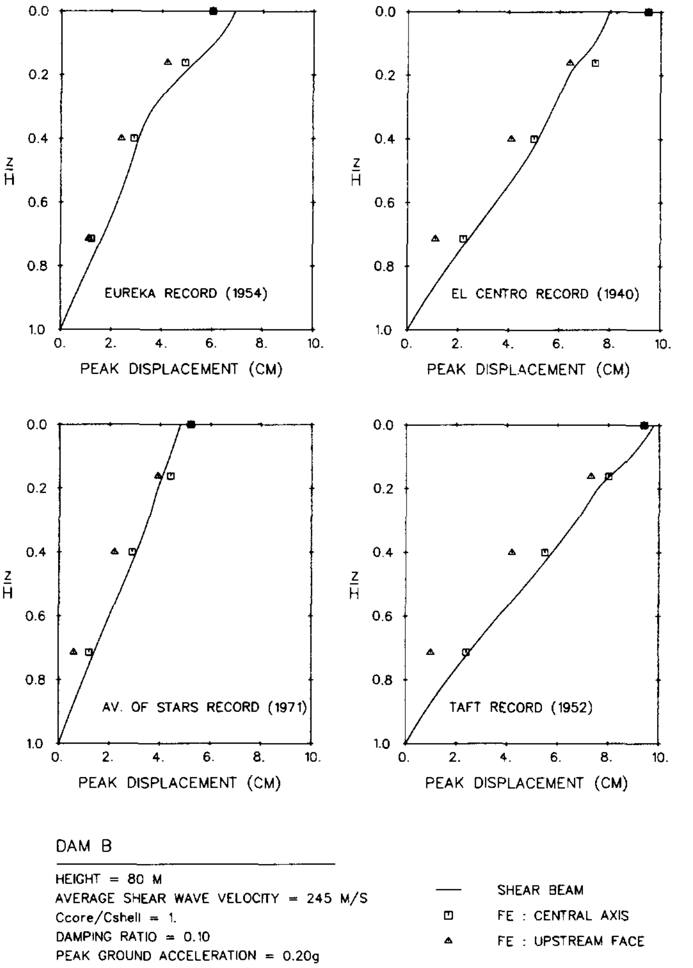

Fig. 14. Dam B: Distribution with depth of peak displacements from SB and FE analyses

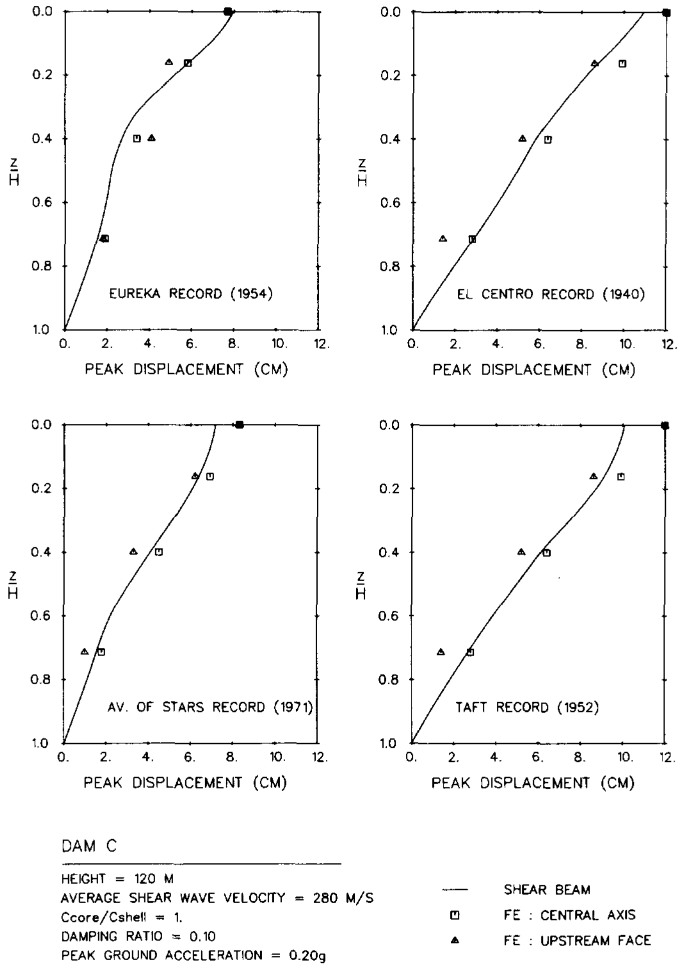

Fig. 15. Dam C: Distribution with depth of peak displacements from SB and FE analyses

The crest amplifications $AF(0)$ from equation (33) ($\lambda=0$) is plotted in Fig. 8a as a function of $a_0=\omega H/\bar{C}$, for seven values of the inhomogeneity parameter, $m=0$, 2/5, 1/2, 4/7, 2/3, 3/4 and 1, and a single value of the hysteretic damping ratio $\beta=0.10$. It is evident that, in addition to lower natural frequencies, increasing inhomogeneity leads to: (i) larger amplitudes at the first resonance and (ii) increased relative importance of the higher resonance. Note, however, that for $\lambda=0.50$ (embankment) the crest amplification $AF(\lambda)$ from equation (31) shows no sensitivity to variations in m (Fig. 8b).

The dependence of the amplification function on the depth parameter, $AF(\zeta)$, is illustrated in Fig. 9, for a dam with $m=4/7$ and $\lambda=0$. Notice that the relative importance of the higher resonances diminishes at greater depths from the crest – this is quite natural since the high-frequency 'whip-lash' effect on flexible structures is observed only near the top.

Finally the effect of the hysteretic damping ratio on the crest amplifications is illustrated in Fig. 10.

RESPONSE TO SEISMIC RECORDS: COMPARISON WITH FINITE-ELEMENT ANALYSES

A major attractiveness of the proposed generalized inhomogeneous shear beam (SB) model lies in its simplicity, manifested in the obtained closed-form results shown in Table 7. Thus, the model can be particularly useful in preliminary design calculations when use of more rigorous but quite expensive models (such as those based on plane-strain finite-elements) is not warranted in view of the great uncertainties regarding geometry, material behaviour and excitation, prevailing at this early stage. It would be of interest to investigate the validity of this simple model by comparing its peak seismic response predictions to those computed with a compatible plane-strain finite-element (FE) analysis. An extensive such comparative study is reported herein and in the companion paper by the authors.[1] It may be noted that in a previous publication, Tsiatas and Gazetas,[28] studied the natural periods and mode displacement shapes of five idealized dam cross-sections and found generally good agreement between shear beam and finite-element predictions.

The five dam cross-sections studied here are portrayed in Fig. 11. They are typical of modern earthfill dams, all having upstream and downstream slopes of 2.5:1 and 2.0:1, and heights ranging from 40 m to 120 m. Table 8 contains their fundamental geometric and material characteristics. For both the core and the shell materials of all dams the shear modulus was assumed to be

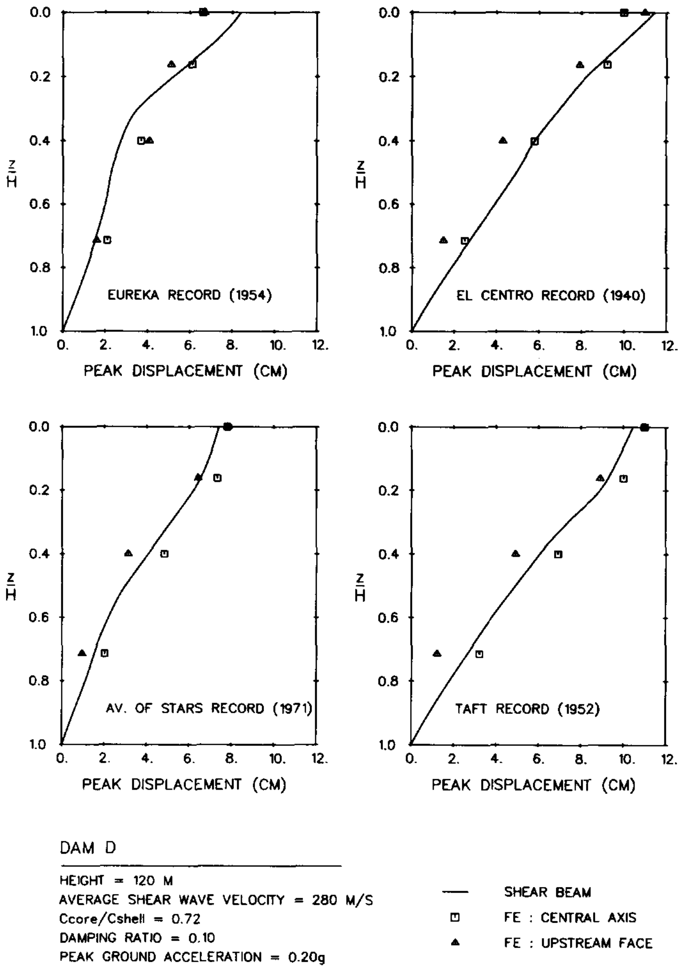

Fig. 16. Dam D: Distribution with depth of peak displacements from SB and FE analyses

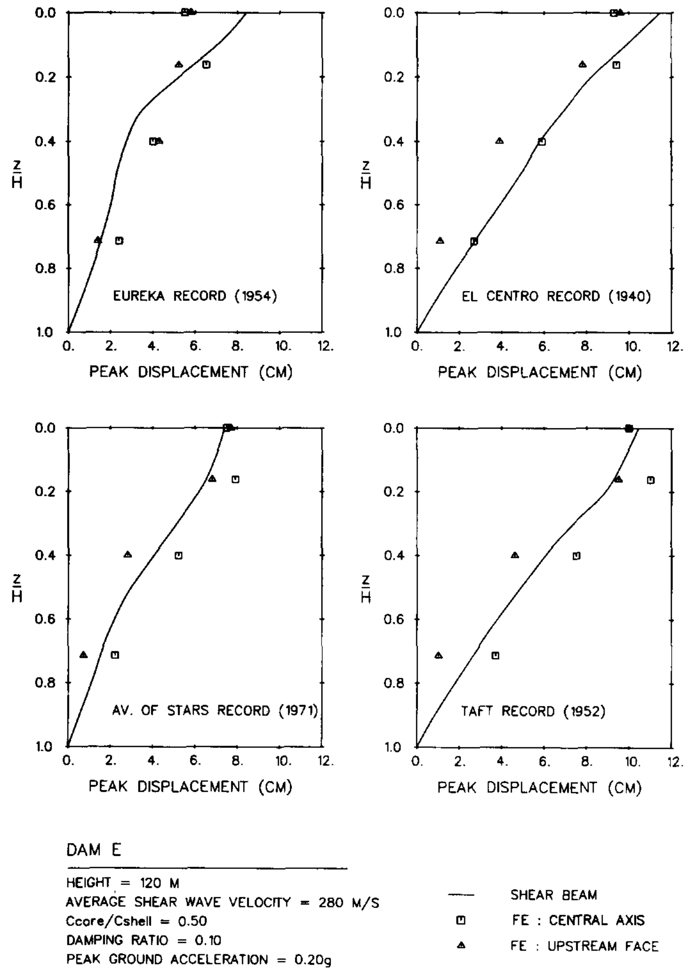

Fig. 17. Dam E: Distribution with depth of peak displacements from SB and FE analyses

proportional to the square-root of the mean pressure, i.e. $\mu = 1/2$ in equation (2). For each cross-section, the distribution with depth of the average (across the width) shear modulus was fitted closely by an expression of the form of equation (3), and thereby the m value of a *consistent* inhomogeneous SB was obtained. For the studied dams m ranged from 0.57 to 0.63.

The fundamental natural periods T_1 of each of the five dams derived from the SB and FE analysis are contrasted in Table 8. It may be concluded that the SB model would only rarely underpredict T_1 by more than 5% – a negligible 'error' in view of the real life uncertainties associated with material properties and frequency content of potential ground excitations. The stiffer behaviour of the SB model should be attributed to the 'suppression' of the vertical degree of freedom, which the actual dam and its FE model enjoy.

To account for the random nature of seismic ground shaking, four historic seismic accelerograms have been selected to excite each of the five dams. These motions were recorded during the earthquake of Eureka 1954, Imperial Valley 1940, San Fernando 1971 and Kern County 1952. Table 9 gives pertinent information on these earthquakes as well as on the specific records used in our analysis. Note that all records have been scaled to a 0.20 g peak ground acceleration. The scaled acceleration histories and the corresponding 10% pseudo-velocity spectra are depicted in Fig. 12. Evidently, the selected records differ substantially in their frequency content, thereby encompassing a reasonably wide range of potential excitations.

Figs. 13–17 plot peak values of horizontal displacements for each of the five dams excited by each of the four records. The continuous lines represent the SB displacements which, being uniform across the dam, are functions of depth only. The plane-strain FE displacements, varying with location across the dam, are depicted as 'data' points; triangles represent displacements of the upstream face, while squares denote displacements of the vertical central axis.

It is worthy of note that in all cases the performance of the inhomogeneous SB model is quite satisfactory. Its peak crest displacements are in most cases within merely 10% of the FE values, with no consistent trend of either over- or under-predicting. Moreover, the SB predicts an attenuation of peak displacements with depth which in the majority of cases lies in between the FE distributions along the face (Δ) and along the central vertical axis ($\square$) of the dam, as in fact is appropriate for shear beam model.

ACKNOWLEDGEMENTS

The authors gratefully acknowledge the financial support by the National Science Foundation, through Grant No. CEE-8205345 to Rensselaer Polytechnic Institute. Thanks are also due to Hermesio Alvarado for the help in collecting the information of Table 1 and to Elsa S. Gazetas in deriving the results of Fig. 2.

REFERENCES

1 Dakoulas P. and Gazetas G. Shear strains and seismic coefficients for dams and embankments, *J. Soil Dynamics & Earthq. Engrg.* (submitted companion paper)

2 Mononobe, H. A. *et al.* Seismic stability of the earth dam, *Proc. 2nd Congress on Large Dams*, Washington, D.C., IV, 1936

3 Hatanaka, M. Fundamental consideration on the earthquake resistant properties of the earth dam, *Bull. No. 11*, Disaster Prevention Research Inst., Kyoto Univ., Japan, 1955

4 Ambraseys, N. N. On the shear response of a two-dimensional truncated wedge subjected to an arbitrary disturbance, *Bull. Seism. Soc. of Am.* 1960, **50**, 45

5 Ambraseys, N. N. and Sarma, S. K. The response of earth dams to strong earthquakes, *Geotechnique* 1967, **17**(3), 181

6 Seed, H. B. and Martin, G. R. The seismic coefficient in earth dam design, *J. Soil Mech. and Found Div.*, ASCE, **92** (SM3)

7 Makdisi, A. M. and Seed, H. B. Simplified procedure for evaluating embankment response. *J. Geot. Engrg. Div.*, ASCE 1979, **105** (GT12), 1427–1434

8 Chopra, A. K. *et al.* Earthquake analysis of earth dams, *Proc. 4th World Conf. Earthq. Engrg.*, Santíago, Chile, 1969

9 Mathur, J. N. Analysis of the response of earth dams to earthquakes. PhD Thesis, Univ. of California, Berkeley, 1969

10 Gazetas, G. A new dynamic model for earth dams evaluated through case histories, *Soils and Foundations* 1981, **21**, 67

11 Gazetas, G. Shear vibrations of vertically inhomogeneous earth dams, *Int. J. of Num. and Anal. Methods in Geomech.* 1982, **6**, 219

12 Gazetas, G. and Abdel-Ghaffar, A. M. Earth dam characteristics from full-scale vibrations, *Prox. X World Conf. Soil Mech. and Found. Engrg.*, Stockholm 1981, 10/7, 207

13 Abdel-Ghaffar, A. M. and Scott, R. F. Analyses of earth dam response to earthquakes, *J. Geotech. Engrg. Div.*, ASCE 1979, **105**, No. GT12, 1379

14 Abdel-Ghaffar, A. M. and Scott, R. F. Comparative study of dynamic response of earth dam, *J. Geotech. Engrg. Div.*, ASCE 1981, **107**, 271–286

15 Oner, M. Shear vibration of inhomogeneous earth dams in rectangular canyons, *Soil Dyn. and Earthq. Engrg.* 1984, **3**(1), 19

16 Hardin, B. and Black, W. Sand stiffness under various triaxial stresses, *J. Soil Mech. and Found. Div.*, ASCE 1966, **92**, (SM2)

17 Hardin, B. and Black, W. Vibration modulus of normally consolidated clay, *J. Soil Mech. and Found Div.*, ASCE, **94** (SM2)

18 Richard, F. E., Hall, J. R. and Wood, R. D. *Vibrations of soil and foundations*, Prentice-Hall, New Jersey, 1970

19 Kokusho, T. and Esashi, Y. Cyclic triaxial test of sands and coarse materials, *Proc. X Int. Conf. Soil Mech. and Found. Engrg.*, Stockholm, 1981

20 Prange, B. Resonant column testing of railroad ballast, *Proc. X Int. Conf. Soil Mech. and Found. Engrg.*, Stockholm, 1981

21 Dezfulian, H. Effects of silt content on dynamic properties of sandy soils, *Proc. of 8th World Conf. on Earth. Engrg.*, San Franciso, Vol. II, 1984

22 Umehara, Y., Ohneda, H. and Matsumoto, K. In-situ soil investigation and evaluation of dynamic properties of sandy soils in very deep sea, *Proc. of 8th World Conf. Earthq. Engrg.*, San Francisco, 1984, Vol. III

23 Moriwaki, V. *et al.* Cyclic strength and properties of tailing slimes, *Dynamic Stability of Tailing Dams*, ASCE 1982

24 Knox, D. P., Stokoe, K. H. II and Kopperman, S. E. Effect of state of stress on velocity of low amplitude shear waves propagating along principal stress directions in dry sand. Geotech. Engrg. Rep. GR82-23, The Univ. of Texas, Austin, 1982

25 Kopperman, S. E., Stokoe, K. H. II and Knox, D. P. Effects of state of stress on velocity of low amplitude compression waves propagating along principal stress direction in dry sand. Geotech. Engrg. Rep. GR82-22, The Univ. of Texas, 1982

26 U.S. Army Corps of Engineers, Omaha District. Chatfield Dam and Reservoir. Design Memorandum No. PC-24, 1968

27 Duncan, J. M., Wong, K. S. and Ozawa, Y. FEADAM: A computer programme for finite element analysis of dams. Report No. UCB/GT/80-02, Univ. of California, Berkeley, 1980

28 Tsiatas, G. and Gazetas, G. Plane-strain and shear beam vibration of earth dams. *J. Soil Dyn. and Earthq. Engrg.* 1982, **1**(4), 150–160